The fourth virial coefficient of anyons

Anders Kristoffersen [a], Stefan Mashkevich [a,b,c], Jan Myrheim [a,c], Kåre Olaussen [a,c]

[a] *Department of Physics, The Norwegian University of Science and Technology, N–7034 Trondheim, Norway*
[b] *Bogolyubov Institute for Theoretical Physics, 252143 Kiev, Ukraine*
[c] *Centre for Advanced Study, Norwegian Academy of Science and Letters, Drammensveien 78, N–0271 Oslo, Norway*

Abstract

We have computed by a Monte Carlo method the fourth virial coefficient of free anyons, as a function of the statistics angle θ. It can be fitted by a four term Fourier series, in which two coefficients are fixed by the known perturbative results at the boson and fermion points. We compute partition functions by means of path integrals, which we represent diagrammatically in such a way that the connected diagrams give the cluster coefficients. This provides a general proof that all cluster and virial coefficients are finite. We give explicit polynomial approximations for all path integral contributions to all cluster coefficients, implying that only the second virial coefficient is statistics dependent, as is the case for two-dimensional exclusion statistics. The assumption leading to these approximations is that the tree diagrams dominate and factorize.

1 Introduction

Anyons are identical particles in the plane characterized by a statistics phase angle θ [1–3]. They may be thought of e.g. as bosons with a "statistics interaction" between two particles which is an angular vector potential proportional to θ/r at a relative distance r. Since this is apparently a long range interaction, it is not immediately obvious that the cluster and virial coefficients should be finite in the thermodynamic limit.

We work out here a path integral representation for the cluster coefficients of anyons, which shows that they are finite. From this point of view the statistics interaction has short range, thus the important property is not the $1/r$ dependence of the vector potential but rather the pointlike nature of the flux. Its range is temperature dependent, however, because it is effective when the particle paths wind around each other, and each path in the path integral represents Brownian motion of a particle in the plane, covering an area inversely proportional to the temperature.

The path integral representation for the cluster coefficients is in fact quite general, and can be applied to anyons in two dimensions, as well as to bosons and fermions in any dimension, interacting by general scalar and vector potentials. The same argument for finiteness holds in general, when the interaction range is sufficiently short.

We have computed numerically the fourth virial coefficient of free anyons, by Monte Carlo evaluation of the four-particle path integrals. We find that it is very nearly constant, i.e. nearly equal to zero for all values of θ. Thus the anyon system is an approximate realization of Haldane's so-called exclusion statistics [4], characterized by a continuously variable parameter g, for which only the second virial coefficient depends on g, in two dimensions [5]. The

correspondence between the two kinds of fractional statistics is given by the relation

$$g = 1 - (1-\alpha)^2 \ , \tag{1}$$

where α is the periodic function of θ defined in eq. (2) below. This correspondence is only approximate, in fact it is known from perturbation theory that the higher virial coefficients of anyons all have a second order variation with θ at the boson and fermion points [6–12]. Our results are consistent with perturbation theory, within the precision obtained.

All observable properties of anyons must be periodic functions of θ with period 2π. Energy eigenvalues and eigenfunctions are analytic functions of θ, except that some are non-analytic at $\theta = 0$, varying like $|\theta|$ rather than θ. Hence the partition functions and all thermodynamic quantities derivable from them will be analytic functions of θ, even at the fermion point $\theta = \pi$, but generally not at the boson point $\theta = 0$.

In the absence of an external magnetic field, the theory is both time reversal and parity invariant if each of these transformations is defined so as to include a change in sign of θ. It follows that energy eigenvalues and thermodynamic quantities, as functions of θ, must be symmetric about $\theta = 0$, hence they are functions of the quantity $\alpha(\theta)$ defined by

$$\alpha(\theta) = \frac{|\theta|}{\pi} \quad \text{for} \quad |\theta| \le \pi \ , \qquad \alpha(\theta + 2\pi) = \alpha(\theta) \ . \tag{2}$$

Note that α is non-analytic in θ at the boson and fermion points, but any even polynomial in α is analytic at the boson point, and any even polynomial in $1-\alpha$ is analytic at the fermion point. An example is the exact second virial coefficient [13, 14, 6],

$$A_2 = \lambda^2 \left[\frac{1}{4} - \frac{1}{2}(1-\alpha)^2 \right] = \lambda^2 \left[-\frac{1}{4} + \frac{g}{2} \right], \tag{3}$$

with g given as in eq. (1). Here $\lambda = \hbar \sqrt{2\pi\beta/m}$ is the thermal wavelength, depending on the mass m and the inverse temperature β. A polynomial in α which is analytic in θ both at the boson and the fermion point, must be constant, because it is a periodic polynomial in θ.

The third virial coefficient is analytic at the boson as well as the fermion point, because it is "supersymmetric", i.e. symmetric under the substitution $\alpha \to 1-\alpha$ [15, 16]. Being analytic everywhere, and periodic in θ with period π, it should be expandable as a rapidly converging power series in $\sin^2\theta$. In fact, very precise numerical calculations [17], see also [18–20], in combination with first and second order perturbative calculations for the complete cluster and virial expansions [6–12], give that

$$A_3 = \lambda^4 \left[\frac{1}{36} + \frac{\sin^2\theta}{12\pi^2} - (1.652 \pm 0.012)\, 10^{-5} \sin^4\theta + \cdots \right]. \tag{4}$$

It may be conjectured that all virial coefficients, with the exception of A_2, are analytic functions of θ. If A_4 is analytic, then it must have the form

$$A_4 = \lambda^6 \left[\frac{\sin^2\theta}{16\pi^2} \left(\frac{1}{\sqrt{3}} \ln\Bigl(\sqrt{3}+2\Bigr) + \cos\theta \right) + \sin^4\theta \,(c_4 + d_4 \cos\theta) + \cdots \right], \tag{5}$$

where the coefficients of the lowest order terms are fixed by perturbation theory at the boson and fermion points. The Monte Carlo results presented here can be fitted to this form with two parameters,

$$c_4 = -0.0053 \pm 0.0003 \ , \qquad d_4 = -0.0048 \pm 0.0009 \ . \tag{6}$$

We estimated the χ^2 per degree of freedom (DOF) to be 3.35 for the two-parameter least squares fit, and 30 for the no-parameter fit to the minimal Fourier series with $c_4 = d_4 = \ldots = 0$. The error estimation is discussed in Section 6 below. We have assumed that the systematic errors can be neglected.

In addition to our numerical results, we derive the following polynomial approximations for the cluster coefficients b_N, valid for any N,

$$\lambda^2 \widetilde{b}_N = \frac{(-1)^{N-1}}{N^2} \prod_{k=1}^{N-1} \left(1 - \frac{N(1-\alpha)^2}{k} \right) = \frac{1}{N^2} \prod_{k=1}^{N-1} \left(1 - \frac{Ng}{k} \right) . \tag{7}$$

One nice property of these polynomials is that they are analytic functions of θ at the fermion point, as the exact cluster coefficients must be. However, they do not give the correct second derivatives at the boson and fermion points, known from perturbation theory, although they do give the correct first derivatives. An alternative way to introduce the same polynomials is to postulate that the second virial coefficient is given by eq. (3), while all higher virial coefficients are independent of α. That is, these are just cluster coefficients for two-dimensional exclusion statistics [21], with the statistics parameter given by (1). The corresponding second order diagrams were identified in ref. [11].

In Sections 2 and 3 below we will review some basic formulae. In Section 4 we describe the Monte Carlo method, emphasizing the difference with respect to ref. [19], where an external harmonic oscillator potential was introduced for regularization. In the method used here, we regularize by introducing a finite area A. In Section 5 we give some analytical results, either exact or approximate. The Monte Carlo results are presented in Section 6, mostly in the form of figures. We conclude in Section 7 with a few comments.

2 The N-anyon partition function

We consider free particles in two dimensions, except that we need to confine them inside a finite area A for purposes of normalization. We might use a square box, but it is simpler to use periodic boundary conditions so that there are no reflecting walls. Note that the periodicity is only used for normalization, and that when we speak about anyons, in the path integral formalism, the only restriction is that the starting points of trajectories should be inside the given area. Otherwise they propagate freely in the plane and not on the torus.

The N-particle partition function is denoted by $Z_N(\beta)$. In particular,

$$Z_1(\beta) = \left[\sum_{n=-\infty}^{\infty} \exp\left(-\pi n^2 \frac{\lambda^2}{A} \right) \right]^2 = \frac{A}{\lambda^2} \left[1 + 2 \sum_{n=1}^{\infty} \exp\left(-\pi n^2 \frac{A}{\lambda^2} \right) \right]^2 , \tag{8}$$

where we have used an identity from ref. [22]. Below we will use only the leading term in the limit $A \to \infty$, that is, we take

$$Z_1(\beta) = \frac{A}{\lambda^2} . \tag{9}$$

The correction terms for finite A are exponential in A. This formula implies the following scaling relation, valid for one free particle in two dimensions,

$$Z_1(L\beta) = \frac{Z_1(\beta)}{L} . \tag{10}$$

By definition, a partition of N is a sequence of non-negative integers, $\mathcal{P} = (\nu_1, \nu_2, \ldots)$, such that $N = \sum_{L=1}^{\infty} \nu_L L$. Let $\mathcal{C}_N$ denote the set of all partitions of N, and let $\mathcal{C} = \bigcup_{N=0}^{\infty} \mathcal{C}_N$ and $\mathcal{C}' = \bigcup_{N=1}^{\infty} \mathcal{C}_N$. In this notation we have that

$$\sum_{\mathcal{P}\in\mathcal{C}} = \sum_{N=0}^{\infty} \sum_{\mathcal{P}\in\mathcal{C}_N} = \sum_{\nu_1=0}^{\infty} \sum_{\nu_2=0}^{\infty} \cdots \sum_{\nu_L=0}^{\infty} \cdots \ . \tag{11}$$

A partition $\mathcal{P}$ of N labels a conjugation class in the symmetric group S_N of permutations of N particles, in such a way that ν_L is the number of cycles of length L. Thus $\mathcal{C}_N$ may be identified with the set of conjugation classes in S_N.

The partition function for N identical particles can in general be expanded as a sum over partitions of N,

$$Z_N(\beta) = \sum_{\mathcal{P}\in\mathcal{C}_N} F_{\mathcal{P}}(\beta)\, B_{\mathcal{P}}(\beta) \ . \tag{12}$$

Here $B_{\mathcal{P}}$ is the contribution from the partition $\mathcal{P}$ to the free particle bosonic partition function,

$$B_{\mathcal{P}}(\beta) = \prod_{L=1}^{\infty} \frac{1}{\nu_L!} \left(\frac{Z_1(L\beta)}{L} \right)^{\nu_L} \ , \tag{13}$$

and the effect of any interaction of the particles, including the anyonic "statistics interaction", is described by a correction coefficient $F_{\mathcal{P}}$.

We consider here the case of free and non-interacting anyons, with an anyon phase angle θ. In the path integral representation of the partition function, $F_{\mathcal{P}}$ can be interpreted as the generating function for the probability distribution of winding numbers [19, 23],

$$F_{\mathcal{P}} = F_{\mathcal{P}}(\beta, \theta) = \sum_{Q=-\infty}^{\infty} P_{\mathcal{P}}(\beta, Q)\, \exp(-\mathrm{i}\theta Q) \ . \tag{14}$$

$P_{\mathcal{P}}(\beta, Q)$ is the probability of the total winding number Q, given the partition $\mathcal{P}$ and given the distribution of paths valid for free bosons at the inverse temperature β.

Further on, we will label a partition by the set of its addends [so $\mathcal{P} = (2, 1, 0, \ldots)$, which is $4 = 2 + 1 + 1$, will be labelled 211]. By eqs. (12)–(13) we have in particular that

$$\begin{aligned}
Z_2(\beta) &= \frac{1}{2} F_{11}\, Z_1(\beta)^2 + \frac{1}{2} F_2\, Z_1(2\beta) \ , \\
Z_3(\beta) &= \frac{1}{6} F_{111}\, Z_1(\beta)^3 + \frac{1}{2} F_{21}\, Z_1(2\beta) Z_1(\beta) + \frac{1}{3} F_3\, Z_1(3\beta) \ , \\
Z_4(\beta) &= \frac{1}{24} F_{1111}\, Z_1(\beta)^4 + \frac{1}{4} F_{211}\, Z_1(2\beta) Z_1(\beta)^2 + \frac{1}{8} F_{22}\, Z_1(2\beta)^2 \\
&\quad + \frac{1}{3} F_{31}\, Z_1(3\beta) Z_1(\beta) + \frac{1}{4} F_4\, Z_1(4\beta) \ .
\end{aligned} \tag{15}$$

Using the scaling (10), and writing Z_N for $Z_N(\beta)$, we get

$$\begin{aligned}
Z_2 &= \frac{1}{2} F_{11}\, {Z_1}^2 + \frac{1}{4} F_2\, Z_1 \ , \\
Z_3 &= \frac{1}{6} F_{111}\, {Z_1}^3 + \frac{1}{4} F_{21}\, {Z_1}^2 + \frac{1}{9} F_3\, Z_1 \ , \\
Z_4 &= \frac{1}{24} F_{1111}\, {Z_1}^4 + \frac{1}{8} F_{211}\, {Z_1}^3 + \frac{1}{32} F_{22}\, {Z_1}^2 + \frac{1}{9} F_{31}\, {Z_1}^2 + \frac{1}{16} F_4\, Z_1 \ .
\end{aligned} \tag{16}$$

For each partition, Z_1 is raised to a power which is the number of cycles.

3 The cluster expansion

The grand canonical partition function is

$$\Xi(\beta,\mu) = 1 + \sum_{N=1}^{\infty} z^N \, Z_N(\beta) \;, \tag{17}$$

where $z = \exp(\beta\mu)$ is the fugacity and μ is the chemical potential. The pressure P is given by the relation

$$\beta P = \frac{\ln \Xi}{A} = \sum_{N=1}^{\infty} b_N z^N \;, \tag{18}$$

where b_N is the N-th cluster coefficient. An immediate consequence is that

$$\Xi = \prod_{N=1}^{\infty} \exp(A b_N z^N) = \sum_{\mathcal{P}\in\mathcal{C}} \prod_{L=1}^{\infty} \frac{\left(A b_L z^L\right)^{\nu_L}}{\nu_L!} \;, \tag{19}$$

and hence,

$$Z_N = \sum_{\mathcal{P}\in\mathcal{C}_N} \prod_{L=1}^{\infty} \frac{(A b_L)^{\nu_L}}{\nu_L!} \;. \tag{20}$$

We are more interested in the inverse relation, which follows from the expansion

$$\ln \Xi = \sum_{\nu=1}^{\infty} \frac{(-1)^{\nu-1}}{\nu} \left(\sum_{L=1}^{\infty} z^L \, Z_L \right)^{\nu} = \sum_{\mathcal{P}\in\mathcal{C}'} (-1)^{\nu-1} (\nu-1)! \prod_{L=1}^{\infty} \frac{\left(z^L \, Z_L\right)^{\nu_L}}{\nu_L!} \;. \tag{21}$$

Here $\nu \equiv \nu(\mathcal{P}) = \sum_{L=1}^{\infty} \nu_L$ is the total number of cycles in the partition $\mathcal{P}$. This gives the cluster coefficients in terms of the N-particle partition functions,

$$A b_N = \sum_{\mathcal{P}\in\mathcal{C}_N} (-1)^{\nu-1} (\nu-1)! \prod_{L=1}^{\infty} \frac{{Z_L}^{\nu_L}}{\nu_L!} \;. \tag{22}$$

In particular,

$$\begin{aligned} A b_1 &= Z_1 \;, \\ A b_2 &= Z_2 - \frac{{Z_1}^2}{2} \;, \\ A b_3 &= Z_3 - Z_2 Z_1 + \frac{{Z_1}^3}{3} \;, \\ A b_4 &= Z_4 - Z_3 Z_1 - \frac{{Z_2}^2}{2} + Z_2 {Z_1}^2 - \frac{{Z_1}^4}{4} \;. \end{aligned} \tag{23}$$

In general we may write

$$A b_N = Z_N + \cdots = \sum_{\mathcal{P}\in\mathcal{C}_N} F_{\mathcal{P}} \, B_{\mathcal{P}} + \cdots = Z_1 \sum_{\mathcal{P}\in\mathcal{C}_N} G_{\mathcal{P}} \, \frac{B_{\mathcal{P}}}{{Z_1}^{\nu}} \;, \tag{24}$$

where we have introduced new coefficients

$$G_{\mathcal{P}} = (F_{\mathcal{P}} + \cdots){Z_1}^{\nu-1} \; . \tag{25}$$

The "$\cdots$" in the last formula represents a sum of terms that are products of "F" coefficients.

One main point of introducing the "G" coefficients is that they tend to a finite limit in the thermodynamic limit $A \to \infty$, as we will prove below. $G_{\mathcal{P}}$ is the "connected part" of $F_{\mathcal{P}}$ for any partition $\mathcal{P}$. The concept of connectedness will also be made more precise below.

With eqs. (9)–(10), we get that

$$\lambda^2 b_N = \sum_{\mathcal{P}\in\mathcal{C}_N} G_{\mathcal{P}} \prod_{L=1}^{\infty} \frac{1}{\nu_L!\, L^{2\nu_L}} \; , \tag{26}$$

and all quantities occurring in this equation are finite in the $A \to \infty$ limit. In particular,

$$\begin{aligned} \lambda^2 b_2 &= \frac{G_{11}}{2} + \frac{G_2}{4} \; , \\ \lambda^2 b_3 &= \frac{G_{111}}{6} + \frac{G_{21}}{4} + \frac{G_3}{9} \; , \\ \lambda^2 b_4 &= \frac{G_{1111}}{24} + \frac{G_{211}}{8} + \frac{G_{22}}{32} + \frac{G_{31}}{9} + \frac{G_4}{16} \; . \end{aligned} \tag{27}$$

We have that $G_1 = F_1 = 1$, $G_N = F_N$ for $N = 2, 3, 4, \ldots$, and

$$\begin{aligned} G_{11} &= (F_{11} - 1)Z_1 \; , \\ G_{111} &= (F_{111} - 3F_{11} + 2){Z_1}^2 \; , \\ G_{21} &= (F_{21} - F_2)Z_1 \; , \\ G_{1111} &= (F_{1111} - 4F_{111} - 3{F_{11}}^2 + 12F_{11} - 6){Z_1}^3 \; , \\ G_{211} &= (F_{211} - 2F_{21} - F_2F_{11} + 2F_2){Z_1}^2 \; , \\ G_{22} &= (F_{22} - {F_2}^2)Z_1 \; , \\ G_{31} &= (F_{31} - F_3)Z_1 \; . \end{aligned} \tag{28}$$

For bosons and fermions the probability generating functions can be factorized as

$$F_{\mathcal{P}} = \prod_{L=1}^{\infty} {F_L}^{\nu_L} \; , \tag{29}$$

where $F_L = 1$ for bosons and $F_L = (-1)^{L-1}$ for fermions. This factorization implies that

$$\Xi = \sum_{\mathcal{P}\in\mathcal{C}} \prod_{L=1}^{\infty} \frac{1}{\nu_L!} \left(\frac{z^L F_L Z_1(L\beta)}{L} \right)^{\nu_L} = \prod_{L=1}^{\infty} \exp\left(\frac{z^L F_L Z_1(L\beta)}{L} \right) , \tag{30}$$

which gives the cluster coefficient

$$b_N = \frac{F_N Z_1(N\beta)}{NA} = \frac{(\pm 1)^{N-1}}{N^2\lambda^2} \; . \tag{31}$$

Thus, for bosons and fermions $G_N = F_N = (\pm 1)^{N-1}$, while $G_{\mathcal{P}} = 0$ for every partition $\mathcal{P}$ containing two or more cycles.

4 The Monte Carlo method

We may use the Monte Carlo method in order to compute numerically the coefficient $G_{\mathcal{P}}$ for a given partition $\mathcal{P}$ representing a conjugation class in the symmetric group S_N. For that purpose we represent $G_{\mathcal{P}}$ as a path integral over all paths inducing one given permutation represented by $\mathcal{P}$,

$$G_{\mathcal{P}} Z_1 = \mathcal{N}_{\mathcal{P}} \int \mathcal{D}(\boldsymbol{r}_1(\tau), \ldots, \boldsymbol{r}_N(\tau)) \exp\left(-\frac{S}{\hbar}\right) g_{\mathcal{P}} \ . \tag{32}$$

Here $\boldsymbol{r}_j(\tau)$ is the path of particle j, as a function of the imaginary time τ, and S is the free particle action in imaginary time,

$$S = \sum_{j=1}^{N} \int_0^{\hbar\beta} \mathrm{d}\tau \ \frac{m}{2} \left| \frac{\mathrm{d}\boldsymbol{r}_j(\tau)}{\mathrm{d}\tau} \right|^2 \ . \tag{33}$$

We include the Gaussian factor $\exp(-S/\hbar)$ as part of the integration measure, so that it is the integrand $g_{\mathcal{P}}$ alone that represents the interaction of the particles, and we include a normalization factor $\mathcal{N}_{\mathcal{P}}$ so that $G_{\mathcal{P}} = {Z_1}^{\nu-1}$ if $g_{\mathcal{P}} = 1$ identically. Note that $\mathcal{N}_{\mathcal{P}}$ is then finite (i.e. A independent), since the path integral is proportional to ${Z_1}^{\nu}$ when $g_{\mathcal{P}} = 1$. Note also that this path integral representation is actually very general, and can be applied to any N-particle system with (short range) interactions in any dimension, not just to the N-anyon system considered here.

To see what the integrand $g_{\mathcal{P}}$ looks like in our case, let us take the partition 2+1+1 of 4 as an example. A closed path in the four-particle configuration space interchanges the positions of two particles, say particles 1 and 2, and takes the remaining two particles back to their starting points. The total winding number Q is the sum of six pairwise winding numbers,

$$Q = Q_{12} + (Q_{13} + Q_{23}) + (Q_{14} + Q_{24}) + Q_{34} \ . \tag{34}$$

Note that Q_{12} is an odd integer and Q_{34} an even integer (remember that the winding numbers are defined such that a complete revolution corresponds to the winding number 2), whereas $Q_{13}, Q_{23}, Q_{14}, Q_{24}$ are in general non-integer, because particles 1 and 2 do not return to their starting positions. However, the sums $Q_{(12)3} = Q_{13} + Q_{23}$ and $Q_{(12)4} = Q_{14} + Q_{24}$ are even integers. Hence Q is an odd integer. Let I be any subscript, and introduce the notation

$$e_I = 1 + f_I = \exp(-\mathrm{i}\theta Q_I) \ . \tag{35}$$

In order to compute the coefficient $G_{211} Z_1 = (F_{211} - 2F_{21} - F_2 F_{11} + 2F_2) {Z_1}^3$ we take the integrand to be

$$\begin{aligned} g_{211} &= e_{12}\, e_{(12)3}\, e_{(12)4}\, e_{34} - e_{12}\, e_{(12)3} - e_{12}\, e_{(12)4} - e_{12}\, e_{34} + 2e_{12} \\ &= e_{12} \left(f_{(12)3}\, f_{(12)4}\, f_{34} + f_{(12)3}\, f_{(12)4} + f_{(12)3}\, f_{34} + f_{(12)4}\, f_{34} \right) \ . \end{aligned} \tag{36}$$

For example, we compute $F_{211} {Z_1}^3$ by integrating

$$\exp(-\mathrm{i}\theta Q) = e_{12}\, e_{(12)3}\, e_{(12)4}\, e_{34} \ , \tag{37}$$

and we compute $2F_{21} {Z_1}^3$ by integrating

$$\exp(-\mathrm{i}\theta(Q_{12} + Q_{(12)3})) + \exp(-\mathrm{i}\theta(Q_{12} + Q_{(12)4})) = e_{12}\, e_{(12)3} + e_{12}\, e_{(12)4} \ . \tag{38}$$

The second line of eq. (36) may be represented diagrammatically as

$G_{211}Z_1 =$  . (39)

The particles are represented as points (filled circles). The two-cycle is represented by e_{12} in the integrand and by a circle connecting two particles in the corresponding diagram. Each factor f_I in the integrand is drawn as a single straight line in the diagram. Note that we should draw *labelled* graphs to represent the four terms in eq. (36). But since the value of a graph is independent of the labelling, it is more natural to draw unlabelled graphs and include instead integer coefficients counting the number of ways each graph can be labelled. Hence the factor 2 in front of the last graph.

In a similar way we find the diagrammatic representation

$G_{1111}Z_1 =$ 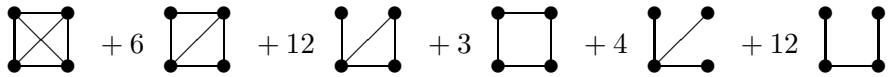 . (40)

The coefficient in front of each diagram is again the number of inequivalent ways of labelling the nodes of the graph. We may also write

$G_{22}Z_1 =$  , $G_{31}Z_1 =$  . (41)

We see that only connected diagrams contribute to the cluster coefficients. It follows that the latter are finite in the limit $A \to \infty$. Indeed, any path gives a non-zero contribution to the path integral represented by some diagram only if for every line in the diagram, the corresponding winding number is non-zero. The probability for this to happen for a connected diagram goes to zero as $(\lambda^2/A)^{\nu-1}$ when $A \to \infty$, since every L-cycle path gives a Gaussian distribution of points which essentially covers only a finite area, proportional to λ^2. Here ν is the number of cycles, and $\nu - 1$ is the minimum number of links in a connected graph with ν nodes. The factor $A^{-\nu+1}$ cancels exactly the divergence of the factor ${Z_1}^{\nu-1}$ included in the definition of $G_{\mathcal{P}}$, eq. (28).

The general meaning of the relations between the F and G coefficients should now be obvious. $F_{\mathcal{P}}$ is a sum of both connected and disconnected diagrams, whereas $G_{\mathcal{P}}$ is the part of the sum including only the connected diagrams. For example, the relation

$$F_{211}{Z_1}^3 = G_{211}Z_1 + 2G_{21}G_1{Z_1}^2 + G_2G_{11}{Z_1}^2 + G_2G_1G_1{Z_1}^3 \,, \tag{42}$$

which follows from (28), is represented as

$F_{211}{Z_1}^3 =$ 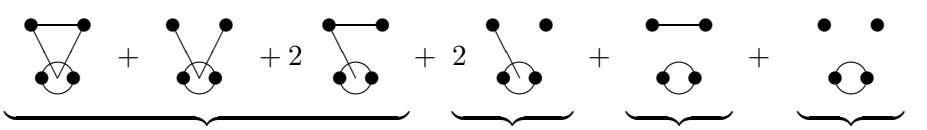 (43)

$G_{211}Z_1$ $\quad 2G_{21}G_1{Z_1}^2$ $\quad G_2G_{11}{Z_1}^2$ $\quad G_2G_1G_1{Z_1}^3$

It is the last term that dominates in the thermodynamic limit, but it is G_{211} only that contributes to the cluster coefficient. Thus, as usual, the grand partition function is a sum of all diagrams but the thermodynamic potential is a sum of connected diagrams [24].

The Monte Carlo method consists in generating random paths according to the Gaussian distribution of paths valid for bosons [19]. Each four-particle path is closed over the imaginary

time interval $\hbar\beta$, in the sense that the final configuration is identical to the initial one, but with the particle positions interchanged by a permutation belonging to the class $\mathcal{P} \subset S_N$. Consider the partition $2+1+1=4$, as in the example above. Then particles 1 and 2 should interchange positions, while particles 3 and 4 should return to their starting points. We take, arbitrarily, the starting point for the path of particle 1 to be at the origin, this is then also the ending point for particle 2. Equivalently, it is the ending point for particle 1 over the imaginary time interval $2\hbar\beta$. The starting point for particle 2, equal to the position of particle 1 after half the imaginary time interval $2\hbar\beta$, can then be generated according to a Gaussian distribution around the origin. The starting and ending point for particle 3 is generated according to a flat distribution inside a square area A centered on the origin. Similarly for particle 4.

For each four-particle path generated we count the winding numbers Q_{12}, $Q_{(12)3}$, $Q_{(12)4}$, Q_{34} and increment a histogram $n(Q)$ in the following way. We compute the total winding number Q and add 1 to $n(Q)$, this takes care of the integrand $e_{12}\, e_{(12)3}\, e_{(12)4}\, e_{34}$. We subtract 1 from $n(Q_{12}+Q_{(12)3})$, in order to take care of the integrand $-e_{12}\, e_{(12)3}$. Similarly, we subtract 1 from $n(Q_{12}+Q_{(12)4})$ and from $n(Q_{12}+Q_{34})$, and we add 2 to $n(Q_{12})$. Finally, G_{211} is the Fourier transform of the histogram $n(Q)$, multiplied by the normalization factor ${Z_1}^2/n$, where n is the total number of four-particle paths generated. The net contribution to the histogram vanishes if more than one of the three winding numbers $Q_{(12)3}$, $Q_{(12)4}$ and Q_{34} is zero, and this is what ensures a finite limit as $A \to \infty$ for the computed G_{211}.

5 Exact and approximate polynomials

The first cluster coefficient, with our definition, is $b_1 = 1/\lambda^2$. The exact result for the second cluster coefficient of free anyons is

$$\lambda^2 b_2 = \frac{G_{11}}{2} + \frac{G_2}{4} = \frac{1}{2}\,(1-\alpha)^2 - \frac{1}{4}\ . \tag{44}$$

Since G_{11} is even and G_2 is odd under the substitution $\alpha \to 1-\alpha$, this implies that

$$G_{11} = \alpha(\alpha-1)\ , \qquad G_2 = F_2 = 1-2\alpha\ . \tag{45}$$

It is further known that the third virial coefficient,

$$A_3 = -2\,\frac{b_3}{{b_1}^3} + 4\,\frac{{b_2}^2}{{b_1}^4}\ , \tag{46}$$

is even under $\alpha \to 1-\alpha$. The odd part of $-2b_3/{b_1}^3$, which is $-\lambda^4 G_{21}/2$, therefore has to cancel the odd part of $4{b_2}^2/{b_1}^4$, which is $\lambda^4 G_{11} G_2$. This condition gives another exact result,

$$G_{21} = 2F_2\, G_{11}\ . \tag{47}$$

One further result [25], which is exact according to the perturbative calculation of ref. [26], is

$$F_L = \prod_{k=1}^{L-1} \left(1 - \frac{L\alpha}{k}\right)\ . \tag{48}$$

Our Monte Carlo results for single cycles of length $L \leq 4$ are consistent with this formula, which is a check of our Monte Carlo calculation as well as of the perturbative calculation.

Another way to compute $G_2 = F_2$, G_{11} and G_{21} is to impose an external harmonic oscillator potential to make the energy spectrum discrete, and then take the zero frequency limit. Only energy levels depending linearly on α contribute to these three quantities. The computation of $G_L = F_L$ for $L > 2$ is much more non-trivial, and in fact the only known method is perturbation theory, because also states with non-linear α dependence contribute.

This is about as far as one can get with exact results. However, in the diagrammatic expansions shown above, one may argue quite generally that the tree graphs are expected to dominate, because every additional line in a diagram represents another factor of the type $f_I = \exp(-\mathrm{i}\theta Q_I) - 1$ in the integrand, with Q_I an even integer. This factor vanishes when $Q_I = 0$, which will happen with a certain probability which is definitely non-zero, and even if it does not vanish it will often have an absolute value smaller than 1. Furthermore, one may argue that the path integral represented by a tree graph should approximately factorize in the same way as its integrand. These two assumptions, of tree diagram dominance and factorization, lead in a not entirely trivial way to the following polynomial approximation for the general coefficient $G_{\mathcal{P}}$,

$$G_{\mathcal{P}} \simeq \widetilde{G}_{\mathcal{P}} = N^{\nu-2}\, {G_{11}}^{\nu-1} \prod_{L=1}^{\infty} (LF_L)^{\nu_L} \ . \tag{49}$$

There is a factor F_L for every cycle of length L, a factor $L_1 L_2 G_{11}$ for every single line connecting two different cycles of lengths L_1 and L_2 (each L-factor counts the number of ways the line can be connected to the cycle), and there is a sum over all $\nu^{\nu-2}$ possible ways to connect the cycles into a tree graph. It is perhaps not obvious how this leads to eq. (49); a simple way to understand the connection is by looking at low order examples: Consider the case of 3 cycles of lengths L_1, L_2, and L_3. They can be connected to a tree graph in 3 possible ways. This gives a coefficient

$$\begin{aligned} &F_{L_1} F_{L_2} F_{L_3} \left(L_1 L_2 G_{11}\, L_2 L_3 G_{11} + L_2 L_3 G_{11}\, L_3 L_1 G_{11} + L_3 L_1 G_{11}\, L_1 L_2 G_{11}\right) \\ &= (L_1 + L_2 + L_3)\, {G_{11}}^2 \prod_{i=1}^{3} L_i F_{L_i}, \end{aligned}$$

which agrees with eq. (49) since $L_1 + L_2 + L_3 = N$. We should point out that eq. (49) was first derived empirically as an approximate representation of the Monte Carlo results.

Special cases where these polynomial formulae are exact, as already mentioned, are the cyclic coefficients $G_L = F_L$, as well as G_{11} and $G_{21} = 2F_2\, G_{11}$. In the three-particle case there is one approximate polynomial,

$$\widetilde{G}_{111} = 3{G_{11}}^2 \ . \tag{50}$$

The four-particle approximate polynomials are:

$$\widetilde{G}_{1111} = 16{G_{11}}^3 \ , \quad \widetilde{G}_{211} = 8F_2{G_{11}}^2 \ , \quad \widetilde{G}_{22} = 4{F_2}^2 G_{11} \ , \quad \widetilde{G}_{31} = 3F_3 G_{11} \ . \tag{51}$$

The polynomial approximations for the G coefficients imply the polynomial approximations for the cluster coefficients given in eq. (7), and those imply in turn that the virial coefficients are independent of the statistics, except for the second coefficient (see Appendix). These polynomials (7) are characteristic of two-dimensional exclusion statistics with statistics parameter (1).

6 Monte Carlo results

In the Monte Carlo integration one has to choose a suitable value for the dimensionless parameter A/λ^2, making a compromise between systematic and statistical errors. We want the limit $A/\lambda^2 \to \infty$, but if we take A/λ^2 too large, we get no statistics. As we have seen, one randomly generated four-particle path contributes to the numerical path integral only if the paths of all four particles wind around each other as one cluster. This necessary condition implies that the systematic errors for large but finite A/λ^2 are exponentially small, since the maximum distance that one particle wanders away from its starting point, has a Gaussian distribution. The exponential convergence for the G coefficients is similar to, although not directly related to, the convergence for Z_1.

Exponential convergence means that one should use one single value of A/λ^2, as large as practically useful, rather than use two or three values and extrapolate. We used the following values,

$$\text{partition } 1{+}1{+}1{+}1{:} \qquad \frac{1}{2\pi\, 0.05} = 3.183\ , \tag{52}$$

$$\text{partition } 2{+}1{+}1{:} \qquad \frac{1}{2\pi\, 0.03} = 5.305\ , \tag{53}$$

$$\text{partitions } 2{+}2 \text{ and } 3{+}1{:} \qquad \frac{1}{2\pi\, 0.01} = 15.915\ . \tag{54}$$

Typically, two to five out of 1000 generated four-particle paths gave non-zero contributions for these partitions. We have generated $1.7\,10^6$ paths for the partition $1+1+1+1$, $16.4\,10^6$ for $2+1+1$, $1.5\,10^6$ for $2+2$, $17.6\,10^6$ for $3+1$, and finally 397 000 paths for the partition 4.

The computed G coefficients are plotted in the Figures 1 to 5, as functions of α. In each case the polynomial approximation, as discussed in the previous Section, is subtracted, and the resulting curve is marked "Re(MC) − polynomial". Because of the statistical errors, the Monte Carlo generated curve has also a non-zero imaginary part, marked "Im(MC)", which is useful because it indicates the statistical errors in the real part. Since the real part is even about $\alpha = 1/2$ and the imaginary part is odd, or vice versa, depending on whether the partition is even or odd, we always plot only the interval $0 \le \alpha \le 1/2$.

Fig. 1 shows the computed G_{1111} with the polynomial $16{G_{11}}^3 = 16(\alpha(\alpha-1))^3$ subtracted. The curve marked "fit" is mostly empirical, and is given by

$$\text{fit} = -\frac{3}{\pi^2}\,\alpha(\alpha-1)\sin^2(\alpha\pi)\ . \tag{55}$$

The figure shows that this is a perfect fit to the Monte Carlo curve, within the statistical uncertainty as indicated by the imaginary part.

Fig. 2 shows the computed G_{211} with the polynomial $8F_2{G_{11}}^2 = 8(1-2\alpha)(\alpha(\alpha-1))^2$ subtracted. The curve marked "fit" is partly empirical, but with a coefficient which is chosen so as to produce the correct second order derivative at $\alpha = 0$ [26]. The formula is:

$$\text{fit} = -\frac{2}{3\pi^2}\,(1-2\alpha)\sin^2(\alpha\pi)\ . \tag{56}$$

Fig. 3 shows the computed G_{22} with $4{F_2}^2 G_{11} = 4(1-2\alpha)^2\alpha(\alpha-1)$ subtracted. The "fit" here is

$$\text{fit} = \frac{2}{\sqrt{3}\pi^2}\,\ln(\sqrt{3}+2)\sin^2(\alpha\pi)\cos^2(\alpha\pi)\ . \tag{57}$$

Fig. 4 shows the computed G_{31} with $3F_3G_{11} = 3(1-3\alpha)(1-(3/2)\alpha)\alpha(\alpha-1)$ subtracted. Here we have chosen

$$\text{fit} = \frac{\sqrt{3}}{4\pi^2}\,\ln(\sqrt{3}+2)\sin^2(\alpha\pi)\cos^2(\alpha\pi)\ . \tag{58}$$

Fig. 5 shows the computed $G_4 = F_4$ with the polynomial $(1-4\alpha)(1-2\alpha)(1-(4/3)\alpha)$ subtracted. The figure supports the claim that the polynomial is exact.

Fig. 6 shows the computed cluster coefficient, $\lambda^2 b_4$ with the polynomial $\lambda^2\widetilde{b}_4$ of eq. (7) subtracted. The parabolas given by the second order perturbation theory at $\alpha = 0$ and $\alpha = 1$ are shown.

Fig. 7 shows the computed virial coefficient, A_4/λ^6. The parabolas given by the second order perturbation theory at $\alpha = 0$ and $\alpha = 1$ are shown. Also plotted are two Fourier series, as given in eq. (5). The curve marked "Fourier 1" has only the two terms required by perturbation theory, i.e. $c_4 = d_4 = \ldots = 0$, whereas the curve marked "Fourier 2" is a least squares fit with the coefficients $c_4 = -0.0053$ and $d_4 = -0.0048$.

The error estimation for the least squares fit requires some comment. We neglected the systematic errors, assuming that they are small. Since the imaginary part of A_4 is zero, by definition, we may estimate the χ^2 per degree of freedom (DOF) for any fit to the real part of the Monte Carlo data by scaling so that $\chi^2/\text{DOF} = 1$ for a comparable fit to the imaginary part. For the no-parameter fit to A_4 with $c_4 = d_4 = \ldots = 0$, we get $\chi^2/\text{DOF} = 30$ by comparison with the no-parameter fit of the exact value zero to the imaginary part. The same scale factor would give $\chi^2/\text{DOF} = 1.18$ for the two-parameter fit to A_4 with c_4 and d_4 as free parameters. However, the two-parameter fit for the real part should rather be compared to a two-parameter fit of the same two terms to the imaginary part, and when we do so, we get instead $\chi^2/\text{DOF} = 3.35$. Comparing the no-parameter and two-parameter fits to the imaginary part, we find a third scale factor such that these two degrees of freedom contribute two to χ^2. The errors of the two fitted parameters c_4 and d_4 for the real part are defined as the changes corresponding to an increase in χ^2 of one, when this third scale factor is included. This gives $c_4 = -0.0053 \pm 0.0003$ and $d_4 = -0.0048 \pm 0.0009$, with uncorrelated errors. We arrive at the clear conclusion that the minimal Fourier series, i.e. with $c_4 = d_4 = \ldots = 0$, is excluded by our Monte Carlo results.

We show Figures 8, 9 and 10 in order to justify partly the polynomial approximations to the tree graphs. The quantity plotted is the contribution $G^{\text{line}}_{L_1L_2}$ to a tree graph of one single line, joining two cycles of lengths (L_1, L_2), in the approximation that the integral represented by the graph factorizes. We claim that this contribution is $L_1L_2G_{11}$, to lowest order. Fig. 8 has $L_1 = 2$ and $L_2 = 1$, and the "fit" which is subtracted from the Monte Carlo data is

$$\text{fit} = 2\alpha(\alpha-1) + 1.07(\alpha(\alpha-1))^2 - 0.3(\alpha(\alpha-1))^3\ . \tag{59}$$

The important information is the coefficient $L_1L_2 = 2$ of the term $G_{11} = \alpha(\alpha-1)$. Fig. 9 has $L_1 = L_2 = 2$, and the "fit"

$$\text{fit} = 4\alpha(\alpha-1) + 5.77(\alpha(\alpha-1))^2 + 2.2(\alpha(\alpha-1))^3 \tag{60}$$

has been subtracted. Fig. 10 has $L_1 = 3$, $L_2 = 1$, and we have subtracted

$$\text{fit} = 3\alpha(\alpha-1) + 2.46(\alpha(\alpha-1))^2\ . \tag{61}$$

The (unphysical) sharp peaks near $\alpha = 0$ in these figures are due to a deficit of high winding numbers in the Monte Carlo simulations.

The last two figures show the splitting of G_{111} into a tree graph and a triangle graph, as the simplest possible example of the contributions of separate graphs. We Monte Carlo generated $40.7\,10^6$ three-particle paths at $A/\lambda^2 = 1/(2\pi\,0.03) = 5.305$. Fig. 11 shows the tree graph contribution $G_{111}^{\rm tree}$, after the following "fit" has been subtracted

$$\text{fit} = 3(\alpha(\alpha-1))^2 - (1/(4\pi^2))\sin^2(\alpha\pi) - 1.41(\alpha(\alpha-1))^3 + 1.8(\alpha(\alpha-1))^4\ . \qquad (62)$$

Fig. 12 shows the triangle contribution $G_{111}^{\rm triangle}$, after subtraction of

$$\text{fit} = 1.41(\alpha(\alpha-1))^3 - 1.8(\alpha(\alpha-1))^4\ . \qquad (63)$$

This example should give some general idea of what errors we make by the two approximations of neglecting loop diagrams and representing the tree graphs by the polynomials of eq. (49). We find no apparent simple mathematical form for the correction terms. For the tree graph alone the leading correction to the polynomial $3(\alpha(\alpha-1))^2$ is of order α^2 at the boson point, and $(\alpha-1)^2$ at the fermion point. The $\sin^2$ form of this correction, as given in eq. (62), reproduces the well known third virial coefficient. In general, we would expect corrections of order α^n and $(\alpha-1)^n$ from graphs with n links, exactly as seen in the present example. However, if we consider not the perturbative orders in α and $\alpha-1$, but rather the magnitudes of the maximal corrections from the tree and triangle graphs, we find that they are comparable.

These considerations suggest that the splitting into graphs does not simplify the problem of calculating the cluster coefficients. One would like for example to develop a perturbation theory for calculating the contributions from separate graphs, but at present we have no such theory.

7 Conclusion

The main results of this paper are the following. The fourth virial coefficient of anyons as computed by the Monte Carlo method is rather well described by a Fourier series consistent with second-order perturbation theory and deviating very little from zero. Our diagram analysis shows in general that all cluster and virial coefficients are finite, and gives, in a certain approximation, a direct correspondence with exclusion statistics. In particular, in this approximation all the virial coefficients starting from the third are constant.

The above approximation, as well as the fact that also the exact third and fourth virial coefficients apparently exhibit quite a regular behavior with α, seem to hint that the interpolation between Bose and Fermi statistics is rather smooth. This is in strong contrast to e.g. the anyon superconductivity phenomenon (non-analytic in θ) believed to take place at low temperatures [28–31]. However, since the dimensionless expansion parameter of the virial series is $x \equiv \lambda^2\rho$, which goes to infinity at zero temperature, it is difficult to predict the low temperature behavior from the first few terms of a virial expansion.

What we *can* test, on the other hand, is the average field approximation [32] on which many of the low temperature predictions are based. In this approximation one replaces the anyon statistical flux with an average magnetic field $\bar{B} = \nu\rho\Phi_0$ (with $\Phi_0 = h/e$ the elementary quantum of flux), and treats the anyons as a collection of non-interacting bosons ($\nu = \theta/\pi$) or fermions ($\nu = \theta/\pi - 1$) in the average magnetic field. This approximation should work equally

well at high and low temperatures. Thus, we may compare the resulting virial expansion with our results. Let $f_\pm(\rho, B)$ be the Helmholtz free energy of non-interacting bosons/fermions in a magnetic field B. Then $f_\pm(\rho, \nu\rho\Phi_0)$ is the free energy of anyons in the average field approximation. This leads to a virial expansion

$$\beta P\lambda^2 = x \mp \frac{1}{4}\,x^2 + \frac{1+3\nu^2}{36}\,x^3 \pm \frac{\nu^2}{16}\,x^4 - \frac{1-100\nu^2+5\nu^4}{3600}\,x^5 + \cdots \tag{64}$$

Not unexpectedly, eq. (64) does not reproduce fermions (bosons) correctly when expanded about bosons (fermions). Implementation of such behavior requires corrections which have to be put in by hand. If this is done (by e.g. a minimal Fourier series), it seems that the average field virial coefficients have a magnitude, and variation with θ, which up to 4th order in x is qualitatively rather similar to our results. Since the average field approximation predicts a thermodynamics with very interesting low temperature behavior, our results do not rule out that this will happen in the exact model as well.

Acknowledgments

We thank the Centre for Advanced Study, Oslo, where this work was initiated, for kind hospitality, financial support and use of computer facilities. This work has received support from the Norwegian Supercomputer Committee through a grant of computing time. The work of A.K. has been partially funded by the Norwegian Research Council under contract No. 100559/410. S.M. acknowledges partial support through grants from the Norwegian Research Council.

A Polynomials for cluster and virial coefficients

In this appendix we will prove the result that the polynomial approximation (7) for the cluster coefficients is equivalent to a virial expansion which is the same as for the two-dimensional free non-relativistic Bose gas, except that the second virial coefficient is given by eq. (3). We will also prove that the polynomial approximation (49) for $G_{\mathcal{P}}$ implies eq. (7).

For simplicity we fix the temperature and choose units such that $\beta = \lambda = 1$. Thus, e.g., the fugacity is $z = \mathrm{e}^{\mu}$. We make use of the expansions

$$\begin{aligned} \rho = \frac{\mathrm{d}P}{\mathrm{d}\mu} &= \sum_{N=1}^{\infty} N b_N\, z^N\,, \\ \frac{\mathrm{d}\mu}{\mathrm{d}\rho} = \frac{1}{\rho}\,\frac{\mathrm{d}P}{\mathrm{d}\rho} &= \sum_{N=1}^{\infty} N A_N\, \rho^{N-2}\,. \end{aligned} \tag{65}$$

We also define

$$\rho_g(\mu) = \sum_{N=1}^{\infty} \frac{z^N}{N} \prod_{k=1}^{N-1} \left(1 - \frac{Ng}{k}\right) = \sum_{N=1}^{\infty} z^N\, \frac{(-1)^{N-1}}{Ng} \binom{Ng}{N}, \tag{66}$$

which is the density corresponding to the cluster coefficients $\widetilde{b}_N$ of eq. (7). For the Bose gas, with $g = 0$, we have $\rho = -\ln(1-z)$. Shifting the second virial coefficient by an amount $\Delta A_2 = g/2$ then gives

$$\mu = \ln\left(1 - \mathrm{e}^{-\rho}\right) + g\rho\,. \tag{67}$$

For every $g > 0$ and every μ, or for $g = 0$ and every $\mu < 0$, this equation clearly has a unique solution $\rho > 0$. We want to prove that the solution is $\rho = \rho_g(\mu)$.

For this purpose we rewrite eq. (67) as

$$\rho = -\ln\left(1 - z\mathrm{e}^{-g\rho}\right) = \sum_{n=1}^{\infty} \frac{z^n}{n}\,\mathrm{e}^{-ng\rho}\,, \tag{68}$$

and apply the following theorem due to Lagrange [27]: The equation $\rho = f(\rho)$ has the solution

$$\rho = \sum_{M=1}^{\infty} \frac{1}{M!} \left(\frac{\mathrm{d}}{\mathrm{d}r}\right)^{M-1} f(r)^M \bigg|_{r=0}\,. \tag{69}$$

This gives

$$\begin{aligned}\rho &= \sum_{M=1}^{\infty} \frac{1}{M!} \sum_{n_1=1}^{\infty} \cdots \sum_{n_M=1}^{\infty} \frac{z^{n_1+\cdots+n_M}}{n_1 \cdots n_M} \left(\frac{\mathrm{d}}{\mathrm{d}r}\right)^{M-1} \mathrm{e}^{-(n_1+\cdots+n_M)gr} \bigg|_{r=0} \\ &= \sum_{N=1}^{\infty} z^N \sum_{M=1}^{N} (-Ng)^{M-1}\, C_{N,M}\,,\end{aligned} \tag{70}$$

where

$$C_{N,M} = \frac{1}{M!} \sum_{n_1=1}^{\infty} \cdots \sum_{n_M=1}^{\infty} \frac{\delta_{n_1+\cdots+n_M,N}}{n_1 \cdots n_M}\,. \tag{71}$$

What we need to show is that

$$\sum_{M=1}^{N} (-Ng)^{M-1}\, C_{N,M} = \frac{(-1)^{N-1}}{Ng} \binom{Ng}{N}\,. \tag{72}$$

It is straightforward to show that

$$\sum_{N=1}^{\infty} z^N \sum_{M=1}^{N} g^M C_{N,M} = \mathrm{e}^{-g\ln(1-z)} - 1 = \sum_{N=1}^{\infty} (-z)^N \binom{-g}{N}\,, \tag{73}$$

and hence,

$$\sum_{M=1}^{N} g^{M-1}\, C_{N,M} = \frac{(-1)^N}{g} \binom{-g}{N}\,. \tag{74}$$

Substituting $g \to -Ng$ we get eq. (72), completing the proof.

We next turn to the cluster coefficients

$$b'_N = \sum_{\mathcal{P}\in\mathcal{C}_N} N^{\nu-2}\, {G_{11}}^{\nu-1} \prod_{L=1}^{\infty} \frac{{F_L}^{\nu_L}}{\nu_L!\, L^{\nu_L}}\,, \tag{75}$$

given by the polynomial approximation in eq. (49). We want to prove that $b'_N = \widetilde{b}_N$.

We may rewrite the above formula as

$$b'_N = \sum_{\nu=1}^{N} \frac{N^{\nu-2}\, {G_{11}}^{\nu-1}}{\nu!} \sum_{n_1=1}^{\infty} \cdots \sum_{n_\nu=1}^{\infty} \delta_{n_1+\cdots+n_\nu,N} \prod_{j=1}^{\nu} \frac{F_{n_j}}{n_j}\,. \tag{76}$$

To evaluate $\rho = \sum_{N=1}^{\infty} N b'_N \, z^N$ we insert eq. (76), interchange the summation order of N and ν and use the relations $N^{\nu-1} z^N = (\mathrm{d}/\mathrm{d}\mu)^{\nu-1} z^N$ and $\sum_{n=1}^{\infty} z^n F_n/n = \rho_\alpha(\mu)$. We find

$$\rho = \sum_{\nu=1}^{\infty} \frac{{G_{11}}^{\nu-1}}{\nu!} \left(\frac{\mathrm{d}}{\mathrm{d}\mu}\right)^{\nu-1} (\rho_\alpha(\mu))^\nu = \sum_{\nu=1}^{\infty} \frac{1}{\nu!} \left(\frac{\mathrm{d}}{\mathrm{d}r}\right)^{\nu-1} (\rho_\alpha(\mu + G_{11} r))^\nu \Bigg|_{r=0} . \tag{77}$$

By the Lagrange theorem, eq. (77) is the solution to the equation $\rho = \rho_\alpha(\mu + G_{11}\rho)$, which, as we saw above, is equivalent to

$$\mu + G_{11}\rho = \ln\left(1 - \mathrm{e}^{-\rho}\right) + \alpha\rho \, . \tag{78}$$

This is precisely eq. (67) with $g = \alpha - G_{11} = 1 - (1-\alpha)^2$, which means that $b'_N = \widetilde{b}_N$ with $\widetilde{b}_N$ as given in eq. (7).

References

[1] J.M. Leinaas and J. Myrheim, Nuovo Cimento 37B (1977) 1.

[2] G.A. Goldin, R. Menikoff and D.H. Sharp, J. Math. Phys. 21 (1980) 650; 22 (1981) 1664.

[3] F. Wilczek, Phys. Rev. Lett. 48 (1982) 1144; 49 (1982) 957.

[4] F.D.M. Haldane, Phys. Rev. Lett. 67 (1991) 937.

[5] S.B. Isakov, D.P. Arovas, J. Myrheim and A.P. Polychronakos, Phys. Lett. A 212 (1996) 299.

[6] A. Comtet, Y. Georgelin and S. Ouvry, J. Phys. A 22 (1989) 3917.

[7] J. McCabe and S. Ouvry, Phys. Lett. B 260 (1991) 113.

[8] A. Comtet, J. McCabe and S. Ouvry, Phys. Lett. B 260 (1991) 372.

[9] D. Sen, Nucl. Phys. B 360 (1990) 397.

[10] A. Dasnières de Veigy and S. Ouvry, Phys. Lett. B 291 (1992) 130.

[11] A. Dasnières de Veigy and S. Ouvry, Nucl. Phys. B 388 (1992) 715.

[12] M. Sporre, J.J.M. Verbaarschot and I. Zahed, Nucl. Phys. B 389 (1993) 645.

[13] D.P. Arovas, R. Schrieffer, F. Wilczek and A. Zee, Nucl. Phys. B 251 (1985) 117.

[14] J.S. Dowker, J. Phys. A18 (1985) 3521.

[15] D. Sen, Phys. Rev. Lett. 68 (1992) 2977.

[16] D. Sen, Phys. Rev. D 46 (1992) 1846.

[17] S. Mashkevich, J. Myrheim and K. Olaussen, Phys. Lett. B 382 (1996) 124.

[18] J. Law, A. Suzuki and R.K. Bhaduri, Phys. Rev. A 46 (1992) 4693.

[19] J. Myrheim and K. Olaussen, Phys. Lett. B 299 (1993) 267.

[20] J. Law, A. Khare, R.K. Bhaduri and A. Suzuki, Phys. Rev. E 49 (1994) 1753.

[21] S.B. Isakov, Int. J. Mod. Phys. A 9 (1994) 2563.

[22] R. Bellman, *A Brief Introduction to Theta Functions*, Holt, Rinehart and Winston, New York (1961).

[23] J. Myrheim, *Anyons*, Notes for the Course on Geometric Phases, ICTP, Trieste (1993).

[24] A. Abrikosov, L. Gorkov, I. Dzyaloshinsky, *Methods of quantum field theory in statistical physics*, Pergamon Press, London and Prentice-Hall, New Jersey (1963), and Dover Publications, Inc., New York (1975).

[25] J. Desbois, C. Heinemann, S. Ouvry, Phys. Rev. D 51 (1995) 942.

[26] A. Dasnières de Veigy, Nucl. Phys. B 458 (1996) 533, and private communication.

[27] E. Goursat, E.R. Hedrick, *A Course in Mathematical Analysis*, Ginn, Boston (1904), vol. 1, pp. 404-405; J.K. Percus, *Combinatorial Methods*, Applied Mathematical Sciences 4, Springer-Verlag, New York–Heidelberg–Berlin (1971).

[28] R.B. Laughlin, Science 242 (1988) 525.

[29] R.B.Laughlin, Phys. Rev. Lett. 60 (1988) 2677.

[30] A.L. Fetter, C.B.Hanna and R.B. Laughlin, Phys. Rev. B39 (1989) 9679.

[31] Y.-H. Chen, F. Wilczek, E. Witten and B.I. Halperin, Int. J. Mod. Phys. B3 (1989) 1001.

[32] F. Wilczek, *Fractional Statistics and Anyon Superconductivity*, World Scientific, Singapore–New Jersey–London–Hong Kong (1990).

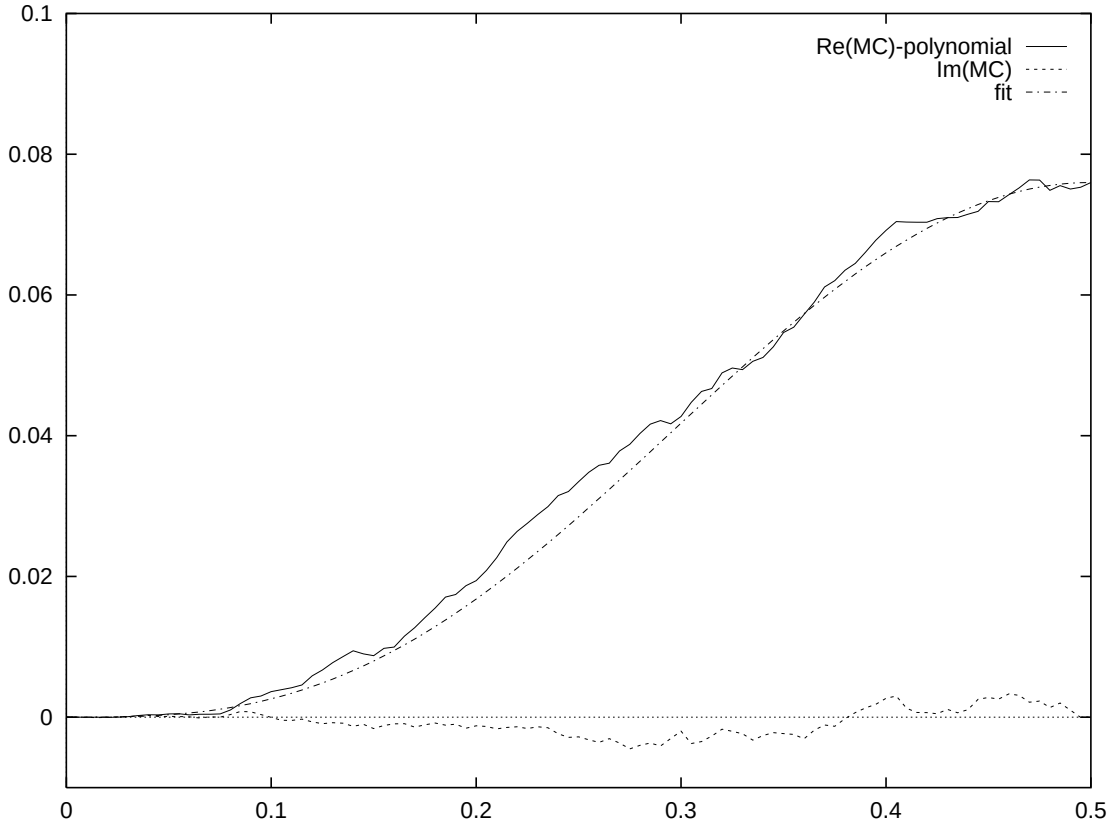

Figure 1: $G_{1111} - 16(\alpha(\alpha-1))^3$ as a function of α. The imaginary part is plotted to indicate the statistical uncertainty of the real part of the Monte Carlo data. Only the interval $0 \leq \alpha \leq 1/2$ is plotted, because of the (anti)symmetry about $\alpha = 1/2$ The curve marked "fit" is given in eq. (55).

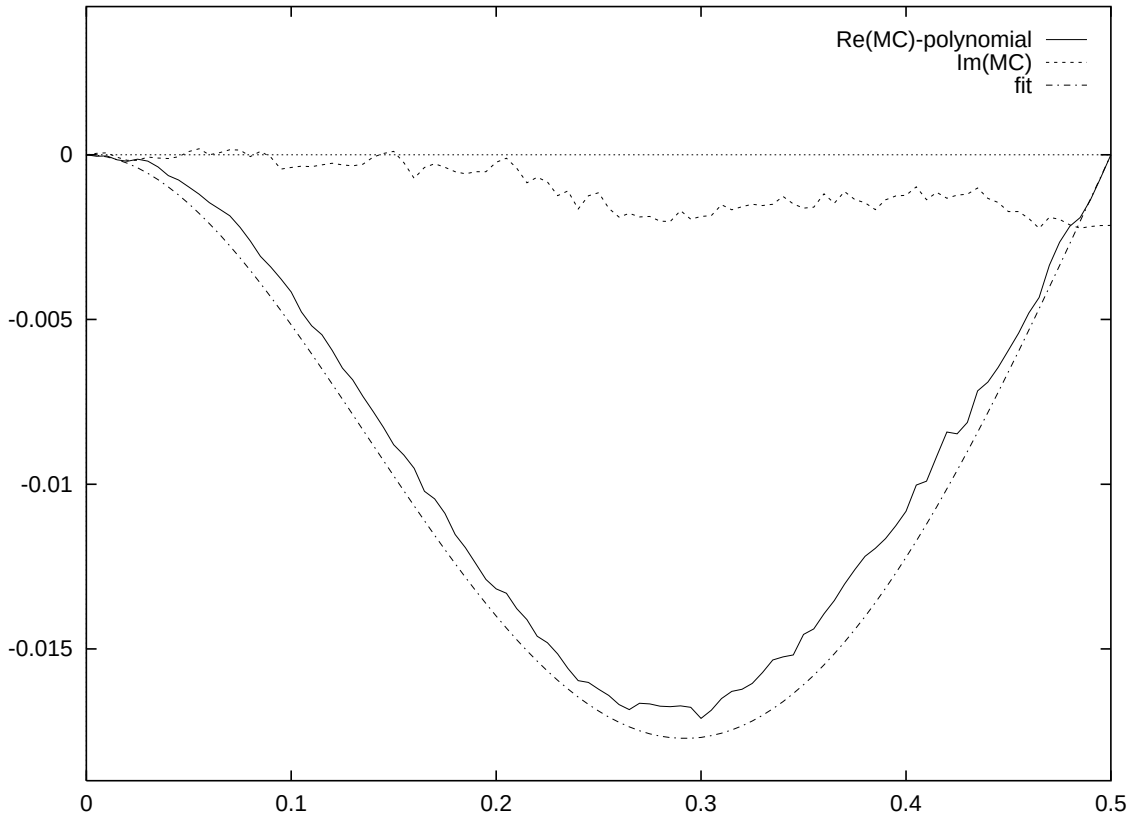

Figure 2: $G_{211} - 8(1-2\alpha)(\alpha(\alpha-1))^2$ versus α. The curve marked "fit" is given in eq. (56).

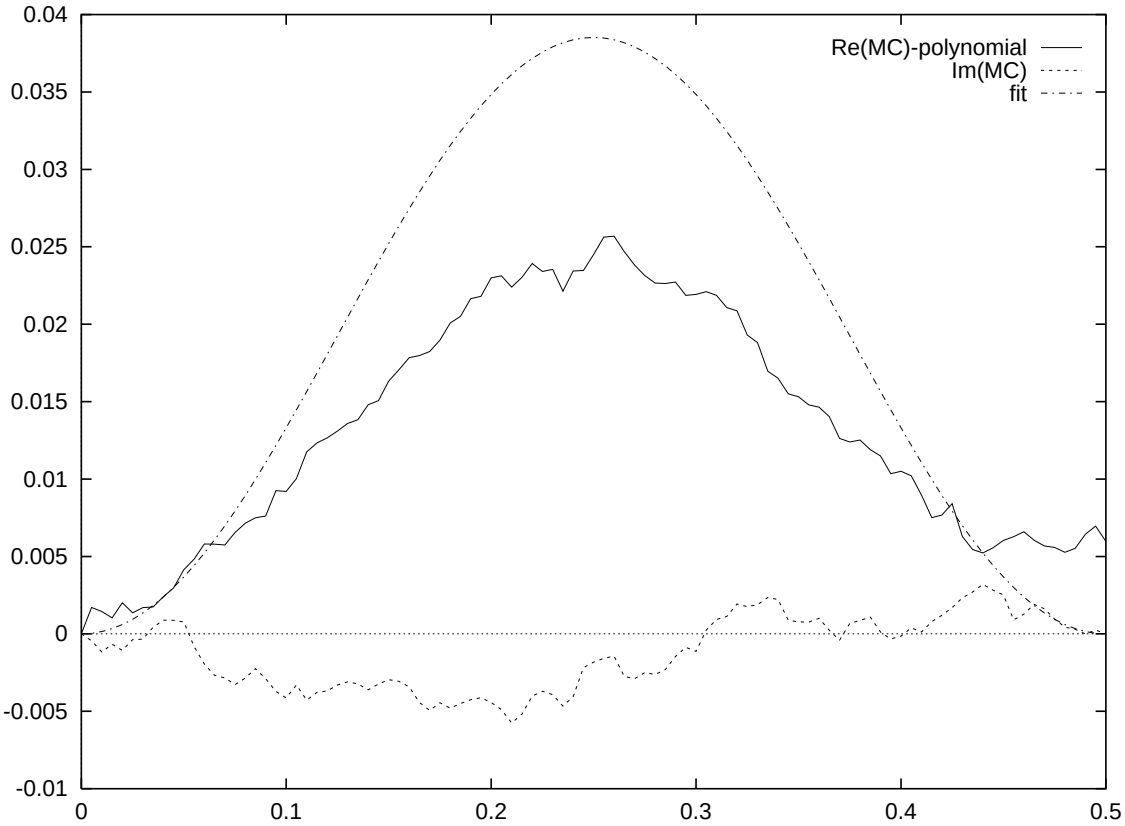

Figure 3: $G_{22} - 4(1-2\alpha)^2\alpha(\alpha-1)$ versus α. The "fit" here is given in eq. (57).

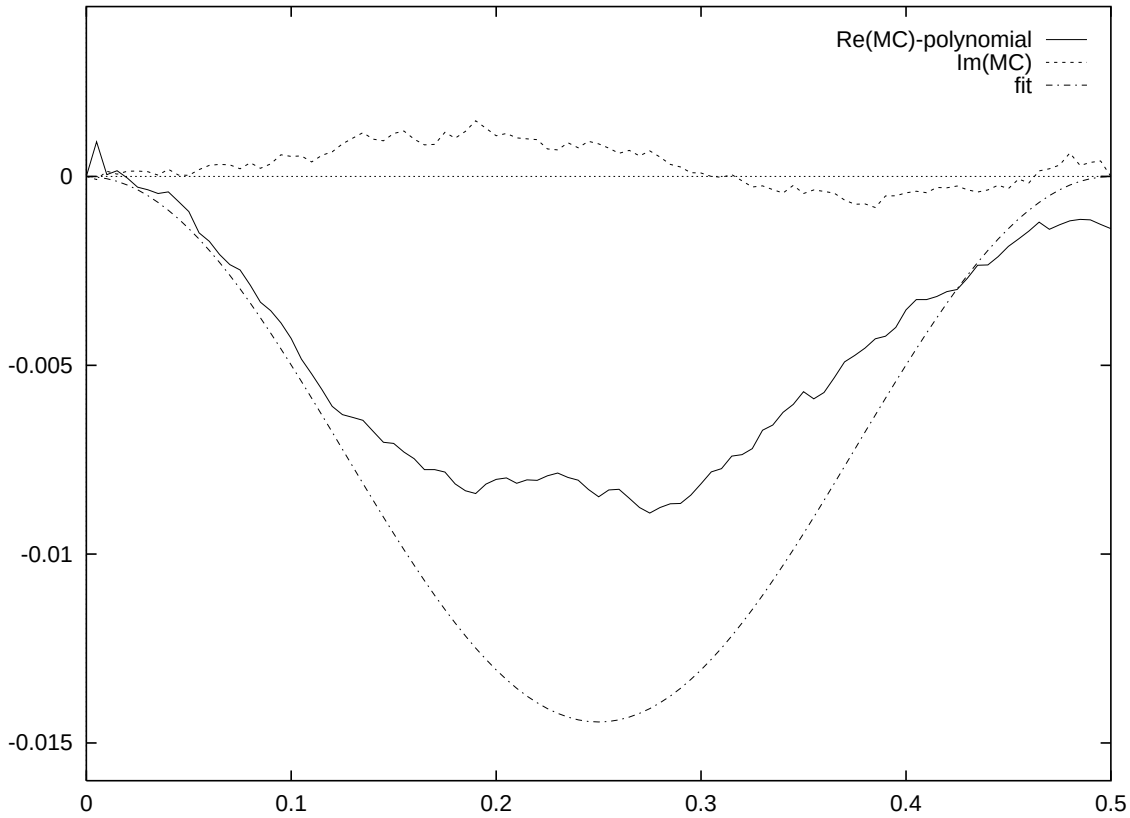

Figure 4: $G_{31} - 3(1-3\alpha)(1-(3/2)\alpha)\alpha(\alpha-1)$ versus α. The "fit" is given in eq. (58).

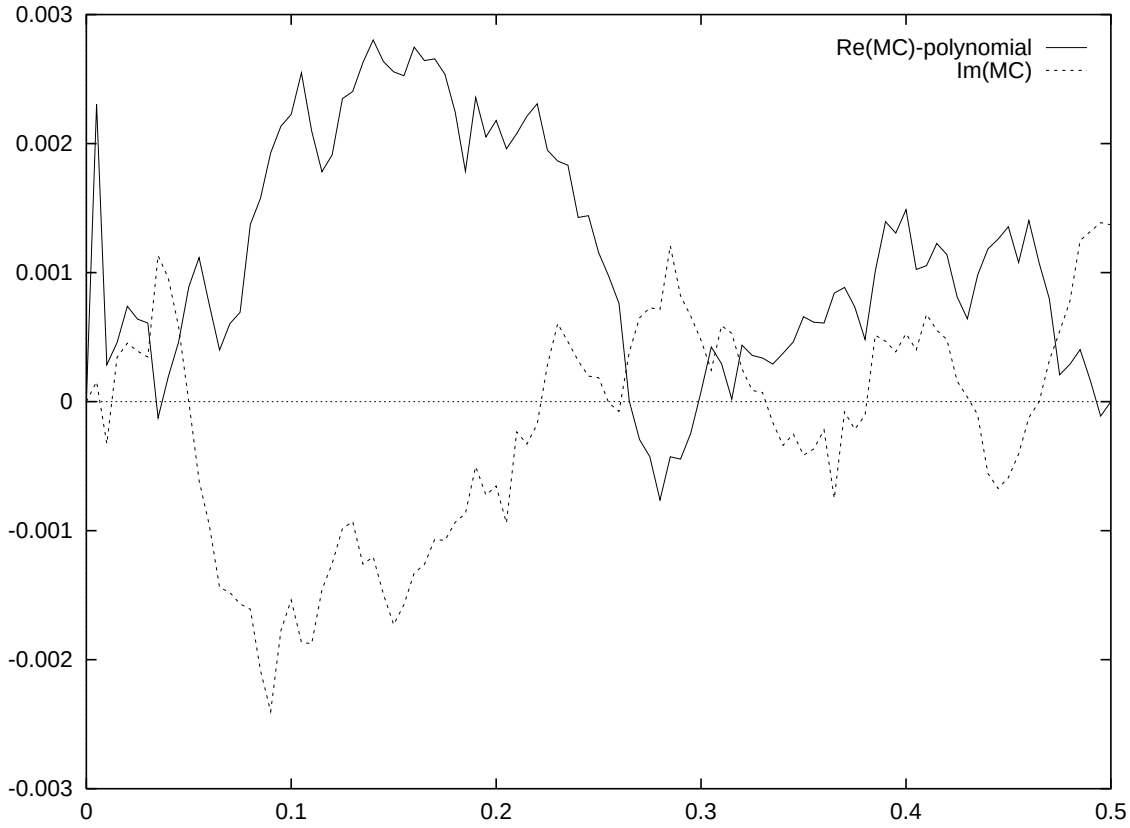

Figure 5: $F_4 - (1-4\alpha)(1-2\alpha)(1-(4/3)\alpha)$ versus α.

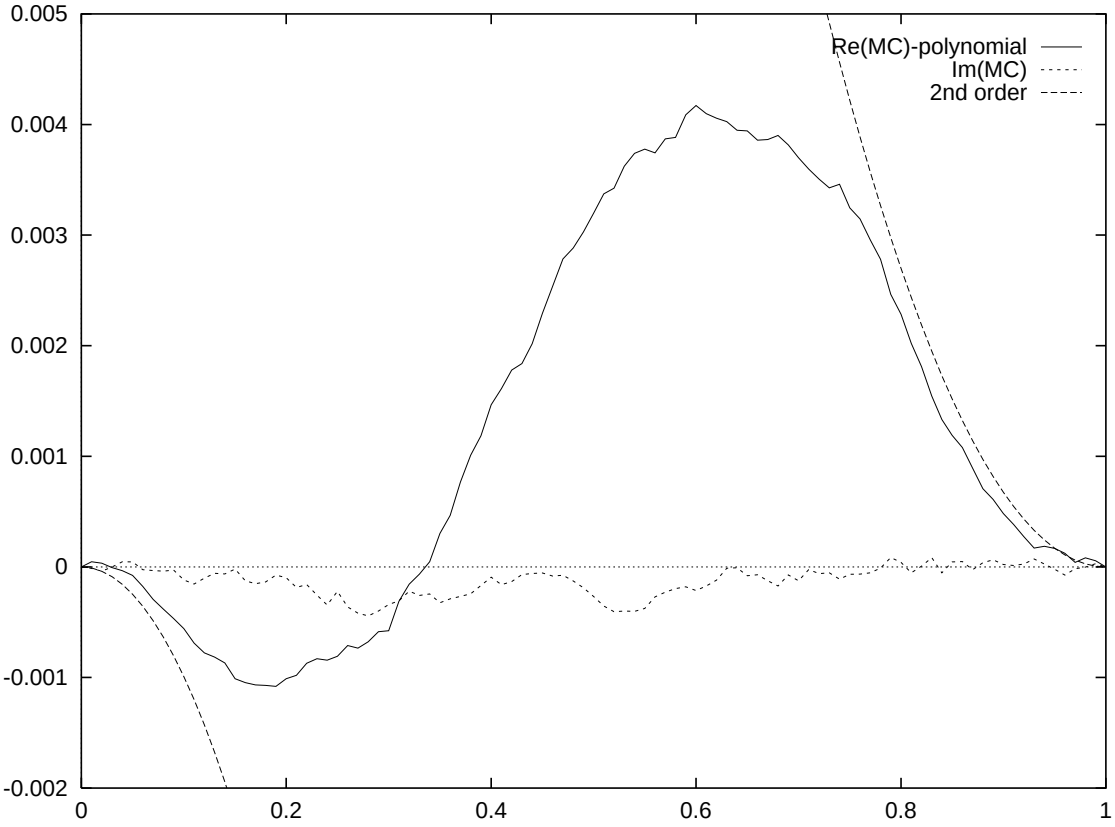

Figure 6: The fourth cluster coefficient minus the polynomial of eq. (7), $\lambda^2(b_4 - \widetilde{b}_4)$, as a function of α. Also shown are the parabolas given by the second order perturbation theory at $\alpha = 0$ and $\alpha = 1$.

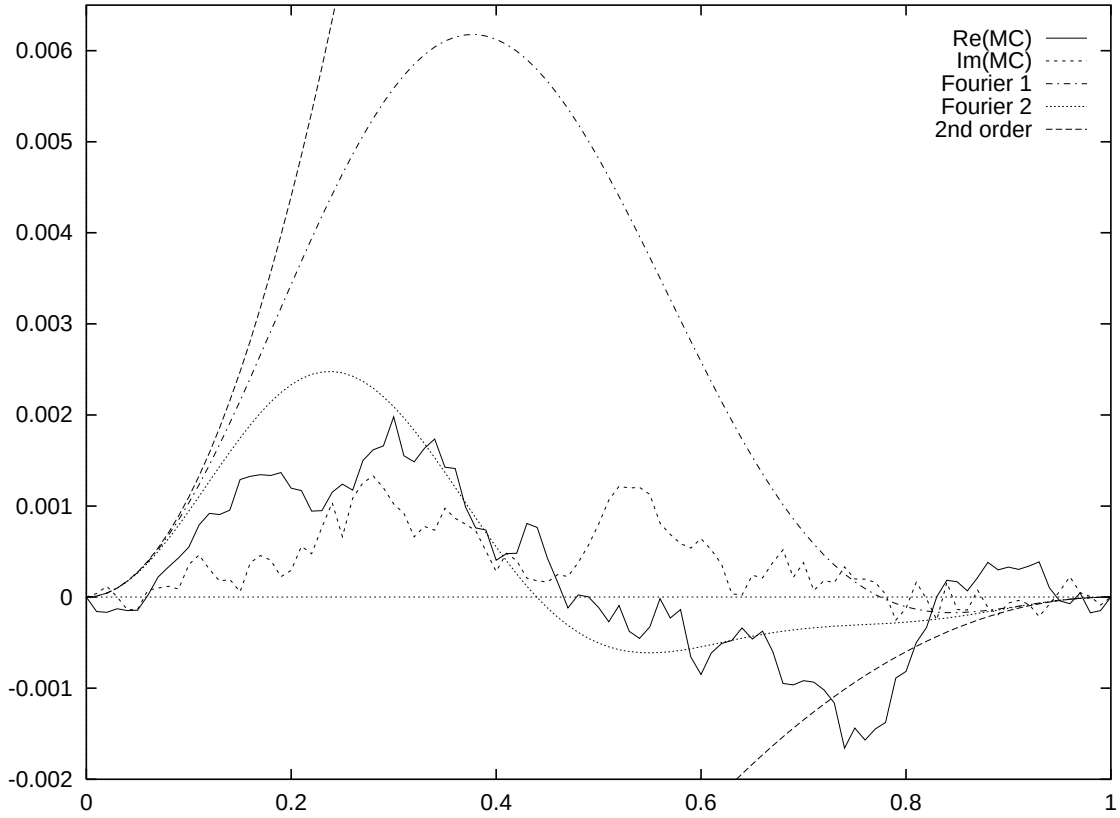

Figure 7: The fourth virial coefficient, A_4/λ^6, as a function of α. Also plotted are the parabolas given by the second order perturbation theory at $\alpha = 0$ and $\alpha = 1$, and two different Fourier series, as given in eq. (5). The curve marked "Fourier 1" has $c_4 = d_4 = \ldots = 0$, whereas "Fourier 2" is the least squares fit with $c_4 = -0.0053$, $d_4 = -0.0048$.

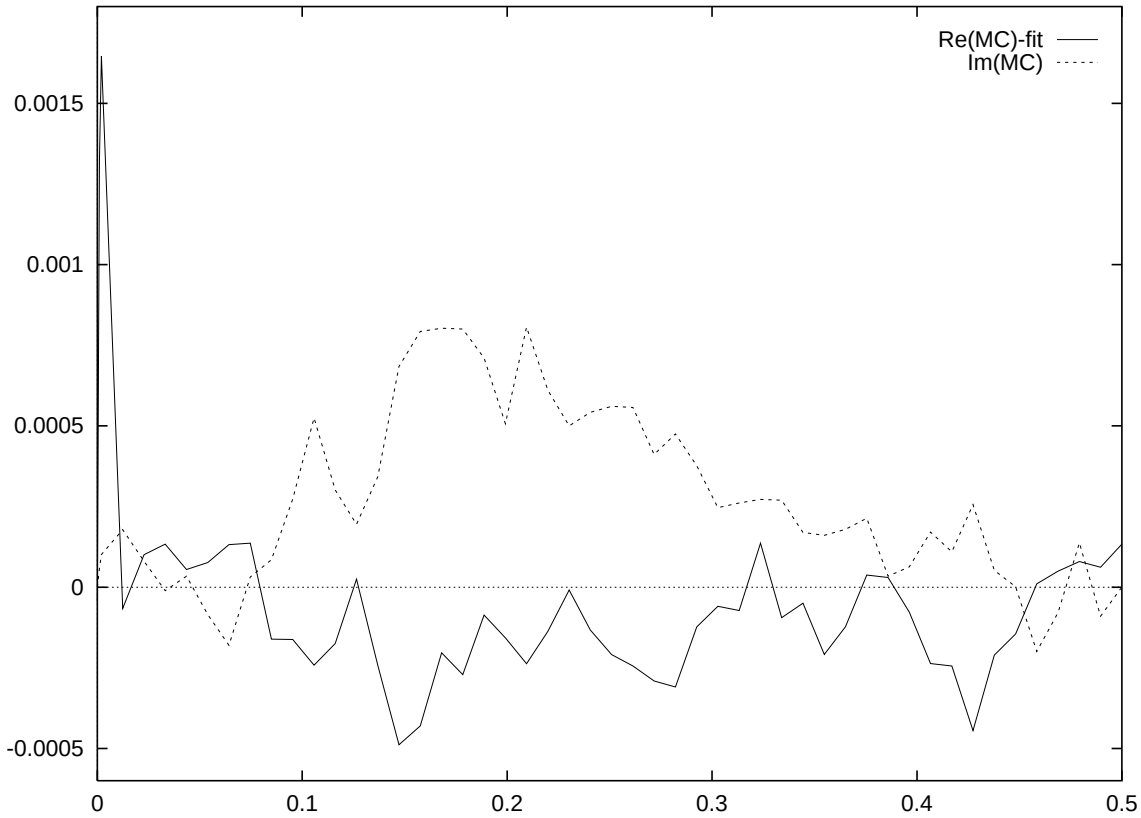

Figure 8: $G_{21}^{\text{line}} - 2\alpha(\alpha-1) - 1.07(\alpha(\alpha-1))^2 + 0.3(\alpha(\alpha-1))^3$ versus α.

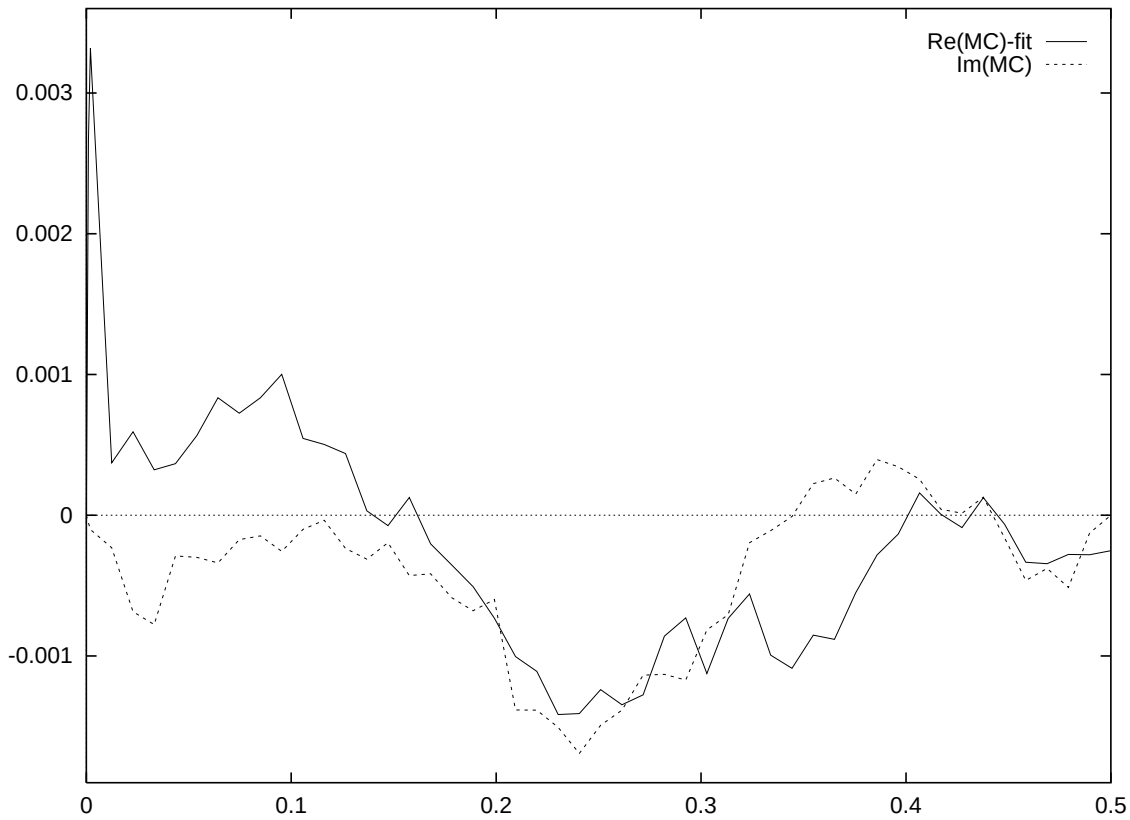

Figure 9: $G_{22}^{\text{line}} - 4\alpha(\alpha-1) - 5.77(\alpha(\alpha-1))^2 - 2.2(\alpha(\alpha-1))^3$ versus α.

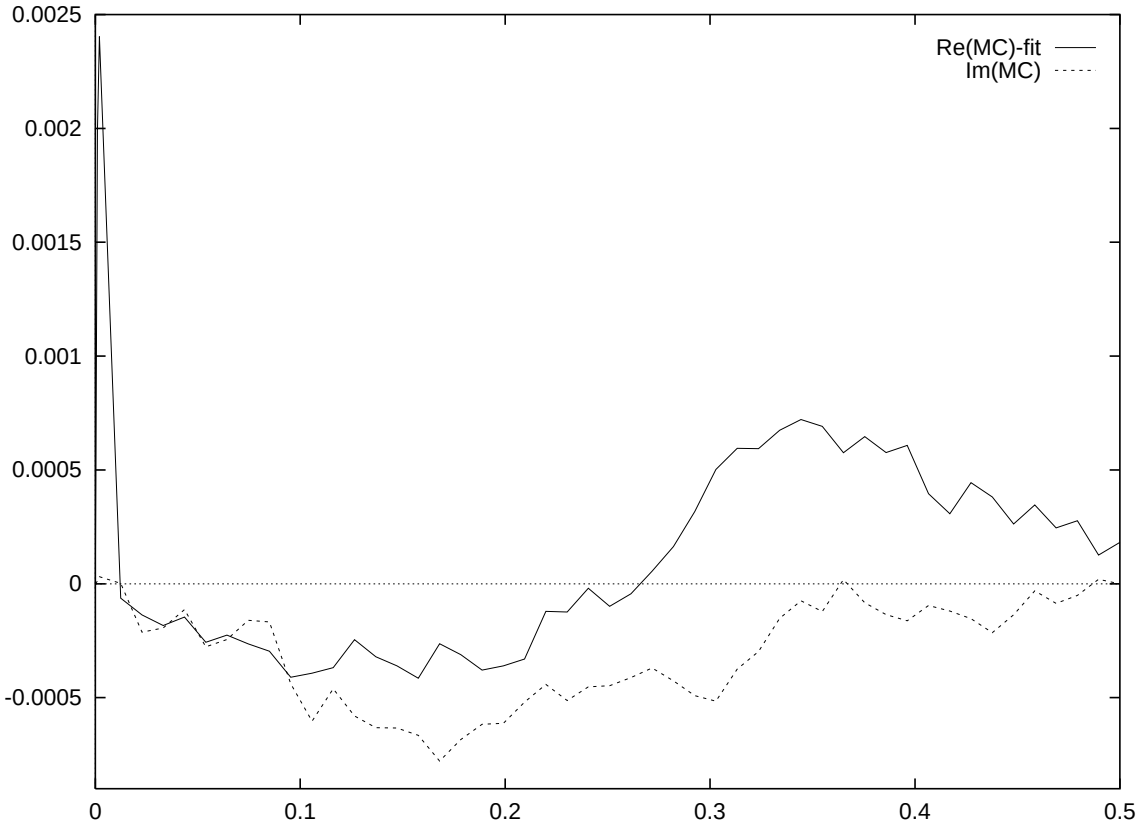

Figure 10: $G_{31}^{\text{line}} - 3\alpha(\alpha-1) - 2.46(\alpha(\alpha-1))^2$ versus α.

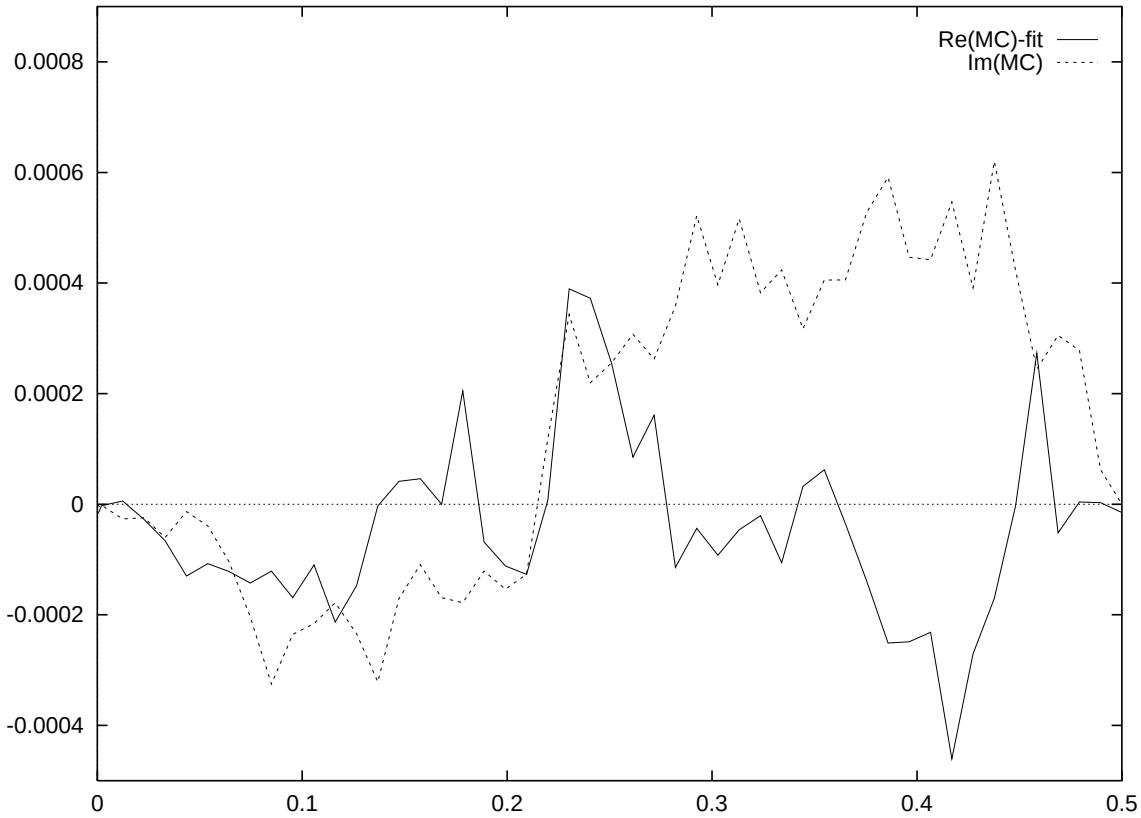

Figure 11: The tree graph contribution $G^{\rm tree}_{111}$ minus the "fit" given in eq. (62).

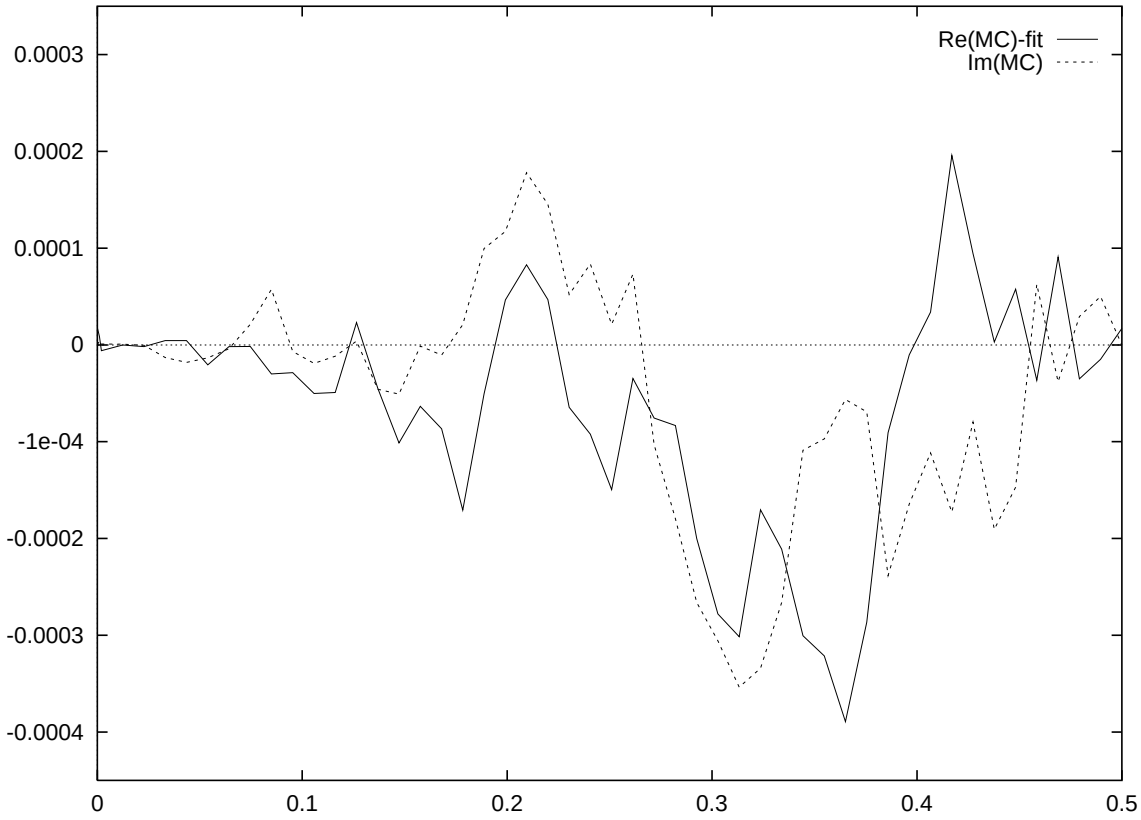

Figure 12: The triangle graph contribution $G_{111}^{\text{triangle}}$ minus the "fit" given in eq. (63).